

Numerical study of turbulent wake flow behind a three-dimensional steep hill

Takeshi Ishihara[†]

*Department of Civil Engineering, University of Tokyo 7-3-1, Hongo, Bunkyo-ku,
Tokyo, 113-8656, Japan*

Kazuki Hibi[‡]

*Wind Engineering Group, Institute of Technology, Shimizu Corp.,
3-4-17, Etchujima, Koto-ku, Tokyo 135-8530, Japan*

Abstract. A numerical investigation on the turbulent flows over a three-dimensional steep hill is presented. The numerical model developed for the present work is based on the finite volume method and the SIMPLE algorithm with a non-staggered grid system. Standard $k-\varepsilon$ model and Shih's non-linear model are tested for the validation of the prediction accuracy in the 3D separated flow. Comparisons of the mean velocity and turbulence profiles between the numerical predictions and the measurements show good agreement. The Shih's non-linear model is found to predict mean flow and turbulence better than the Standard $k-\varepsilon$. Flow patterns have also been examined to explain the difference in the cavity zone between 2D and 3D hills.

Key words: finite volume method; three-dimensional steep hill; turbulent recirculating flow; turbulent models.

1. Introduction

Prediction of the turbulent flows over steep terrain plays a dominant role in many engineering applications such as the safety of structures, extraction of wind energy, pollutant dispersion, wind damage on agriculture and forestry, and aviation safety. However, comparatively fewer investigations have been made of turbulent wake flows behind steep terrain; see, for example, (Coelho and Pereira 1992, Kobayashi *et al.* 1994, Ferreira *et al.* 1995, Kim *et al.* 1997, Utnes and Eidsvik 1996). Prediction accuracy of numerical solutions for mean velocity as well as turbulence in the separated region has not been made fully clear.

This paper aims to provide a detailed numerical study of the separated flows behind a circular hill, having a cosine-squared cross section and a maximum slope of about 32° , and to evaluate the numerical solutions of the equations of motion and the associated turbulence models. In the following section, the numerical model and the discretization procedure are described. Detailed comparisons with experimental data and discussion of the results are presented in Section 3. The final section provides concluding remarks regarding turbulence model for the prediction of the

[†] Associate Professor

[‡] Chief Researcher

turbulent wake flow behind steep terrain.

2. Numerical model

2.1. Governing equations and turbulence model

The Reynolds averaged Navier-Stokes equations and turbulence models Eqs. (1)-(4) are used in the present study, providing information on the mean velocity components u_j (the overbar is dropped for simplicity) along the directions x_j , the static pressure p , turbulence kinetic energy k and its dissipation ε .

$$\frac{\partial \rho u_j}{\partial x_j} = 0 \quad (1)$$

$$\frac{\partial \rho u_j u_i}{\partial x_j} = -\frac{\partial p}{\partial x_i} + \frac{\partial}{\partial x_j} \left(\mu \frac{\partial u_i}{\partial x_j} - \rho \overline{u'_i u'_j} \right) \quad (2)$$

$$\frac{\partial \rho u_j k}{\partial x_j} = \frac{\partial}{\partial x_j} \left[\left(\mu + \frac{\mu_t}{\sigma_k} \right) \frac{\partial k}{\partial x_j} \right] - \rho \overline{u'_i u'_j} \frac{\partial u_i}{\partial x_j} - \rho \varepsilon \quad (3)$$

$$\frac{\partial \rho u_j \varepsilon}{\partial x_j} = \frac{\partial}{\partial x_j} \left[\left(\mu + \frac{\mu_t}{\sigma_\varepsilon} \right) \frac{\partial \varepsilon}{\partial x_j} \right] - C_{\varepsilon 1} \frac{\varepsilon}{k} \rho \overline{u'_i u'_j} \frac{\partial u_i}{\partial x_j} - C_{\varepsilon 2} \frac{\rho \varepsilon^2}{k} \quad (4)$$

In these equations, ρ is the fluid density and μ is the laminar viscosity. The constants ($C_{\varepsilon 1}$, $C_{\varepsilon 2}$, σ_k , σ_ε) in Eqs. (3) and (4) are assigned to standard values (1.44, 1.92, 1.0, 1.3) (Jones and Launder 1972). The turbulent viscosity μ_t is defined as a function of turbulence kinetic energy and dissipation :

$$\mu_t = \rho C_\mu \frac{k^2}{\varepsilon} \quad (5)$$

The fluctuating velocity components are identified by the turbulent Reynolds stress tensor. The expression of the Reynolds stress is an important factor for successful simulations of the turbulent wake flows. In this study, a nonlinear expression proposed by Shih *et al.* (1995) is used to approximate the Reynolds stress.

$$\overline{u'_i u'_j} = \frac{2}{3} k \delta_{ij} - 2 C_\mu \frac{k^2}{\varepsilon} S_{ij} + 2 C_2 \frac{k^3}{\varepsilon^2} (-S_{ik} \Omega_{kj} + \Omega_{ik} S_{kj}) \quad (6)$$

This expression has several advantages compared to the standard k - ε eddy viscosity model which corresponds to the first two terms on the right-hand side of Eq. (6) with a constant $C_\mu = 0.09$. First, this model is fully realizable (Schumann 1977, Lumley 1978). It will not produce negative energy components and will not violate the Schwarz's inequality between turbulent velocities. Second, the effective eddy viscosity is anisotropic as it should be. The coefficients C_μ and C_2 in the Shih's model are determined from the following relations :

$$C_\mu = \frac{1}{6.5 + A_3^* U^*(k/\varepsilon)}, \quad C_2 = \frac{\sqrt{1 - 9 C_\mu^2 (Sk/\varepsilon)^2}}{1 + 6 S \Omega (k^2/\varepsilon^2)},$$

where

$$\begin{aligned}
 S &= \sqrt{S_{ij}S_{ij}}, & S_{ij} &= \frac{1}{2}\left(\frac{\partial u_i}{\partial x_j} + \frac{\partial u_j}{\partial x_i}\right) \\
 \Omega &= \sqrt{\Omega_{ij}\Omega_{ij}}, & \Omega_{ij} &= \frac{1}{2}\left(\frac{\partial u_i}{\partial x_j} - \frac{\partial u_j}{\partial x_i}\right) \\
 U^* &= \sqrt{S_{ij}S_{ij} + \Omega_{ij}\Omega_{ij}}, & W^* &= \frac{S_{ij}S_{jk}S_{ki}}{S^3} \\
 A_s^* &= \sqrt{6} \cos \phi, & \phi &= \frac{1}{3} \arccos \sqrt{6} W^*
 \end{aligned}$$

2.2. Numerical scheme

In the Cartesian coordinate system x_j ($j = 1, 2, 3$), the governing Eqs. (1)-(4) can be written in the form of general transport equation as

$$\frac{\partial \rho u_j \phi}{\partial x_j} = \frac{\partial}{\partial x_j} \left(\Gamma_\phi \frac{\partial \phi}{\partial x_j} \right) + S_\phi \quad (7)$$

where Γ_ϕ stands for diffusion coefficients and S_ϕ denotes source terms of the governing equations. Table 1 lists the contributions of Γ_ϕ and S_ϕ for each ϕ - equation.

To suit the computation of complex flow, the non-staggered grid system is used. The governing equations are rewritten in the curvilinear coordinate system :

$$\frac{\partial \rho U_j \phi}{\partial \xi_j} = \frac{\partial}{\partial \xi_j} \left(\Gamma_\phi J q_{jk} \frac{\partial \phi}{\partial \xi_k} \right) + JS_\phi \quad (8)$$

where the contravariant velocities (U, V, W) are given by

$$\begin{bmatrix} U \\ V \\ W \end{bmatrix} = J \begin{bmatrix} \xi_x & \xi_y & \xi_z \\ \eta_x & \eta_y & \eta_z \\ \zeta_x & \zeta_y & \zeta_z \end{bmatrix} \begin{bmatrix} u \\ v \\ w \end{bmatrix}$$

Table 1 $\phi, \Gamma_\phi, S_\phi$ for the governing equations

Equation	ϕ	Γ_ϕ	S_ϕ
Mass	1	–	0
Momentum	u_i	μ	$-\frac{\partial p}{\partial x_i} + \frac{\partial}{\partial x_j} (-\rho \overline{u_i' u_j'})$
Turbulence Energy	k	$\mu + \frac{\mu_t}{\sigma_k}$	$-\rho \overline{u_i' u_j'} \frac{\partial u_i}{\partial x_j} - \rho \epsilon$
Dissipation	ϵ	$\mu + \frac{\mu_t}{\sigma_\epsilon}$	$-C_{\epsilon 1} \frac{\epsilon}{k} \rho \overline{u_i' u_j'} \frac{\partial u_i}{\partial x_j} - C_{\epsilon 2} \frac{\rho \epsilon^2}{k}$

the coefficient q_{jk} is

$$q_{jk} = \frac{\partial \xi_j}{\partial x_l} \frac{\partial \xi_k}{\partial x_l}$$

and the Jacobian, J , is defined by

$$J = \frac{\partial(x, y, z)}{\partial(\xi, \eta, \zeta)} = \begin{bmatrix} x_\xi & y_\xi & z_\xi \\ x_\eta & y_\eta & z_\eta \\ x_\zeta & y_\zeta & z_\zeta \end{bmatrix}$$

In this study, finite volume method is used to discretize the governing equations over a non-orthogonal mesh :

$$a_p \phi_P = \sum_{nb} a_{nb} \phi_{nb} + b_\phi, \quad nb = W, E, S, N, B, T \quad (9)$$

where W, E, S, N, B, T indicate west, east, south, north, bottom and top sides of the finite volume, and P denotes the center of the finite volume (see Fig. 1). Here b_ϕ is the source term.

The SIMPLE algorithm (Patankar 1980) is used. The QUICK (Leonard 1979) scheme is employed for the convection terms in the Navier-Stokes equations, the first order upwind difference for the convection terms in the equations of k and ε , and the second-order central difference for the other terms. The Rhie and Chow's PWIM (pressure weighted interpolation method) (Rhie and Chow 1983) is used to avoid pressure-velocity decoupling.

2.3. Boundary conditions

The inlet boundary is located $30H$ upstream of the center of the hill. At this section the influence of the hill may be neglected. The inlet boundary conditions for the velocity components and the turbulence kinetic energy are prescribed according to the experimental data for undisturbed flow (Ishihara and Hibi 1998). The dissipation rate, ε , is calculated by

$$\varepsilon = \frac{C_\mu^{3/4} k^{3/2}}{l}, \quad l = \min(\kappa z_m, \kappa \delta) \quad (10)$$

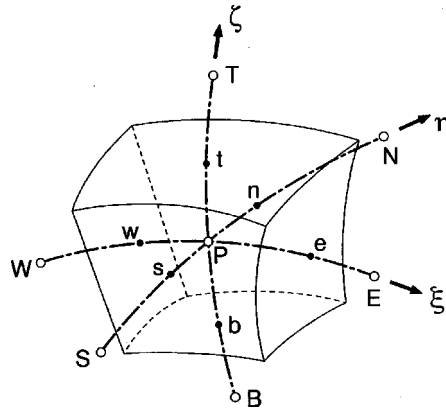


Fig. 1 Typical control volume

Here z_n is the normal distance away from the wall, and δ and κ denote the boundary layer depth and von Karman's constant, respectively.

The boundary conditions used for the velocity are :logrithmic law (Launder and Spalding 1974) on the lower boundary and hill; rigid stress-free on upper and lateral side boundaries and a simple outflow condition of zero gradient on the outlet located $30H$ downstream of the center of the hill. The zero gradient is assumed for the pressure at all boundaries.

The shear stress parallel to the wall is calculated by

$$\tau_w = \frac{\rho \kappa C_\mu^{1/4} k_P^{1/2} U_P}{\ln(z_P/z_0)}$$

Here, z_P is the normal distance away from the wall, U_P represents the velocity component parallel to the wall, and k_P is the turbulence kinetic energy. The subscript P denotes the center of the wall-adjacent cell. z_0 is roughness length and is set to be 0.3 mm according to the experiment (Ishihara and Hibi 1998). This approach is similar to that proposed by Launder and Spalding (1974) for smooth wall, assuming in the wall-adjacent cell a logarithmic velocity profile, a constant-stress layer and local equilibrium of the turbulence. The shear stress τ_w is considered as a drag term to be included in the momentum equations for the wall-adjacent cells.

The cell-averaged production of k , \bar{P}_k , and the dissipation rate, $\bar{\varepsilon}$, are used as the source terms of the transport equation of the turbulence kinetic energy for the wall-adjacent cells. They can be computed from the volume average of P_k and ε of the wall-adjacent cells, and are approximated with a depth average :

$$\bar{P}_k = \frac{1}{2z_P} \int_0^{2z_P} \tau_w \frac{\partial U}{\partial z_n} dz_n = \frac{\tau_w^2}{2z_P C_\mu^{1/4} k_P^{1/2} \kappa \rho} \ln\left(\frac{2z_P}{z_0}\right) \quad (12)$$

$$\bar{\varepsilon} = \frac{1}{2z_P} \int_0^{2z_P} \varepsilon dz_n = \frac{C_\mu^{3/4} k_P^{3/2}}{2z_P \kappa} \ln\left(\frac{2z_P}{z_0}\right) \quad (13)$$

The convective and diffusive wall fluxes for turbulence kinetic energy are set to zero.

The dissipation rate ε is not solved at the wall-adjacent cells, but is prescribed according to local equilibrium:

$$\varepsilon_P = \frac{C_\mu^{3/4} k_P^{3/2}}{z_P \kappa} \quad (14)$$

3. Results and discussion

3.1. Flow configuration

To evaluate the performance of the turbulence model, data obtained from a wind tunnel study (Ishihara and Hibi 1998) are used. The experiment was conducted in a return wind tunnel with a working section of 1.1 m wide, 0.9 m high and 7 m long. The wind speed outside the boundary layer, U_{ref} , was maintained at 5.9 m/s. The simulated turbulent boundary layer was about 0.36 m thick at the point where the hill was mounted and had a surface Reynolds number, $u_* z_0 / \nu$, of 6.4. This implies that the flow was aerodynamically rough and hence independent of the Reynolds number. Measurements were made using split-fiber probes. Calibration procedures have been

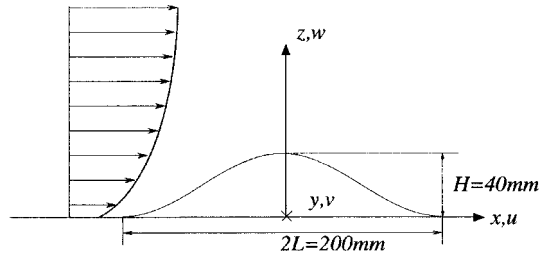


Fig. 2 Coordinate system and notations

described by the authors (Ishihara, Hibi and Oikawa 1999). The velocity profiles on the flat floor at 4.6 m downstream of the contraction exit are adequately represented by the logarithmic law,

$U/u_* = \kappa^{-1} \ln((z-d)/z_0)$, with $u_* = 0.32$ m/s, $z_0 = 0.3$ mm and $d = 3$ mm. Considering that simulated boundary layer has a scale of 1/1000, the equivalent full scale z_0 is 0.3 m, which is characteristic of a forest covered hill.

The model hill has a cosine-squared cross-section and can be expressed as :

$$z_s = \begin{cases} H \cos^2\left(\pi \frac{\sqrt{x^2 + y^2}}{2L}\right), & \sqrt{x^2 + y^2} < L \\ 0 & , \sqrt{x^2 + y^2} \geq L \end{cases} \quad (15)$$

Here, the hill height H is 40 mm and the base radius L is equal to 100 mm. Fig. 2 shows the coordinate system where x , y and z are the streamwise, spanwise and vertical directions, respectively. In the x -direction, zero is the center of hill. A second vertical coordinate $z' = z - z_s$ is also used to denote height above the local surface.

The integration domain has $60H$ length, $20H$ width and $22.5H$ high. Calculation was performed with $70 \times 35 \times 32$ grid nodes in the x -, y - and z -direction, respectively. A uniform grid was used in the cross-wind direction, and a non-uniform grid was adopted in the longitudinal and vertical direction. Typical mesh used in the simulation is presented in Fig. 3.

3.2. Mean flow fields

Predicted profiles of streamwise and vertical velocity at different stations in the central plane of

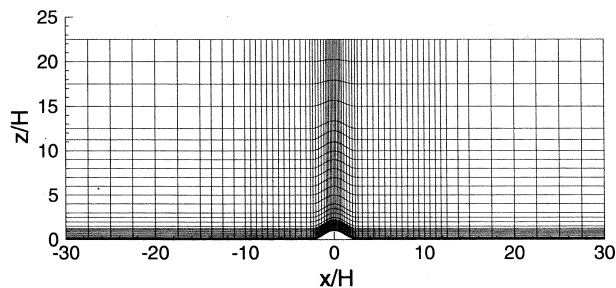


Fig. 3 Typical mesh used in the simulation

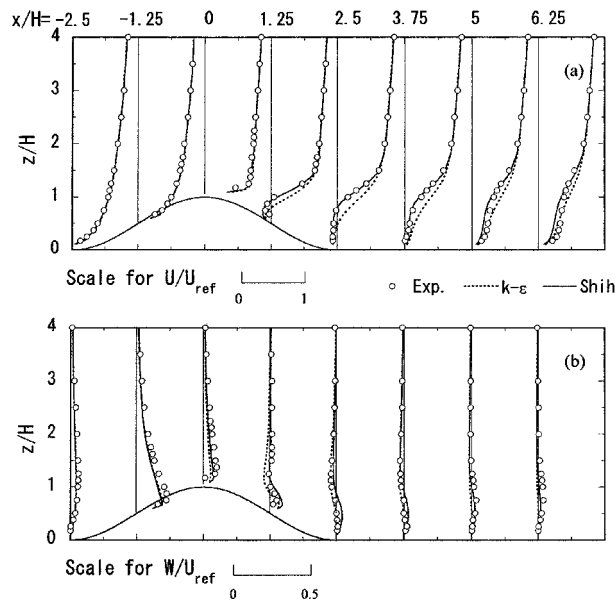


Fig. 4 Comparison of predicted and measured mean velocity profiles in the central plane of the 3D hill: (a) streamwise velocity; (b) vertical velocity

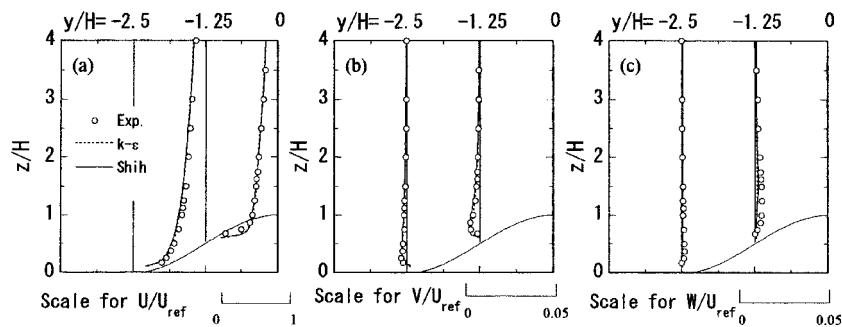


Fig. 5 Comparison of predicted and measured mean velocity profiles in the $x/H=0$ plane: (a) streamwise velocity; (b) spanwise velocity; (c) vertical velocity

the hill are given in Fig. 4. The velocity components are normalized by the free stream velocity U_{ref} . Standard $k-\varepsilon$ model and Shih's nonlinear model yield virtually identical results on the upstream side of the hill. Relatively large differences were obtained inside the separated region, where the predicted streamwise velocity by standard $k-\varepsilon$ was higher than the experimental value. The main reason is presumed to be due to the overestimate of the turbulence kinetic energy in the separated region. The recovery region appears to be represented well by this model, but this is fortuitous and simply due to the premature reattachment. Moreover, the standard $k-\varepsilon$ model fails to reproduce the updraft formed behind the hill. In contrast, the predicted velocity by Shih's nonlinear model is in good agreement with the measurements, except in the region behind the reattaching point where the predictions display a slow recovery.

Fig. 5 shows the vertical profiles of mean velocities in the $x/H=0$ plane. Since the flow doesn't separate at these locations, the standard $k-\varepsilon$ model is also able to give a good agreement with the

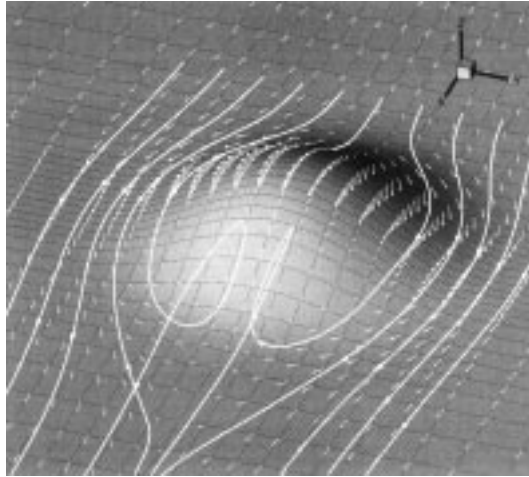


Fig. 6 Traces over the 3D hill

measurements.

To understand how the fluid particles go in and out of the separated region, three-dimensional particle traces were made. Fig. 6 shows that eleven particles start from the upstream foot of the hill. The particles near the central plane pass around behind the hill and enter the separated region. These particles are lifted toward the hilltop by the upward flow on the lee slope of the hill and then escape downstream. This flow pattern is considerably different from that behind the two-dimensional ridge. In order to examine the flow structure behind the three-dimensional hill in detail, mean velocity vectors and flow patterns in some representative cross-sections are depicted in Figs. 7-8.

Fig. 7a shows mean velocity vectors and streamlines in the central plane of the hill. The most striking behavior is that opened streamlines are shown in the three-dimensional wake, while closed sheamlines are revealed in the two-dimensional case (Fig. 7b) (Ishihara and Hibi 2000). The reason why the flow pattern changes can be interpreted using the continuity equation ($\partial u / \partial x + \partial w / \partial z = -\partial v / \partial y$). In the case of two-dimensional separation, the circulating flow must be formed to satisfy the continuity equation. While in the case of three-dimensional separation it is possible to satisfy the continuity equation without the circulating flow, since the spanwise flow exists. Namely, when flow field in the central plane is considered as a two-dimensional field, the term of $-\partial v / \partial y$ becomes a source or a sink in the fictitious two-dimensional field. It becomes a source when $\partial v / \partial y$ is negative and a sink as $\partial v / \partial y$ is positive. In fact, $\partial v / \partial y$ is negative in the lee of the hill. The movement of the flow can be easily observed from the velocity vectors in the parallel surface of the hill.

Fig. 8 illustrates mean velocity vectors and flow pattern in the parallel surface of the hill at $z'/H = 0.025$. Two vortices with the normal (to the hill surface) component of vorticity are observed on the lee slope of the hill. These vortices are sustained by the flows from at least three opposing directions. Clearly a three-way-encounter pattern can only occur in three-dimensional separated regions. With these two vortices, the flow toward the symmetry-plane is formed in the lee of the hill. This flow contributes to the source term in the fictitious two-dimensional field.

Fig. 9 demonstrates mean velocity vectors and flow patterns in the several transverse planes. As expected the spanwise velocity component at the position of $x/H = -2.5$ (Fig. 9a) is everywhere upward and outward as the flow is diverted. These flows generate clockwise vorticity component in

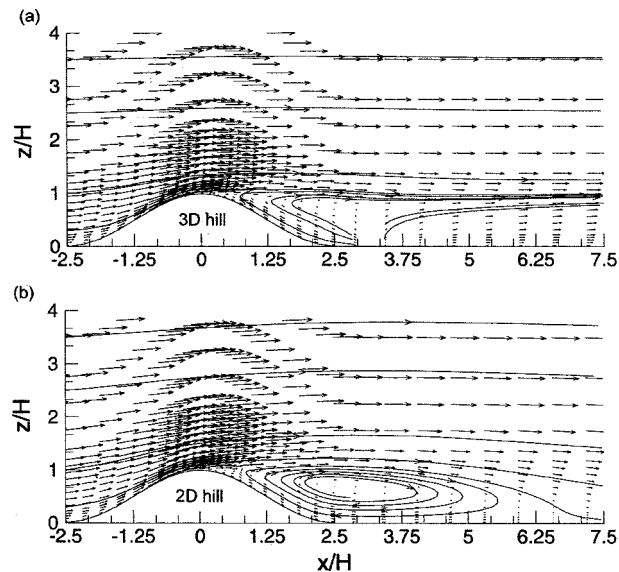


Fig. 7 Comparison of flow patterns behind (a) 3D and (b) 2D hill. The streamlines (solidlines) are superimposed on the mean velocity vectors

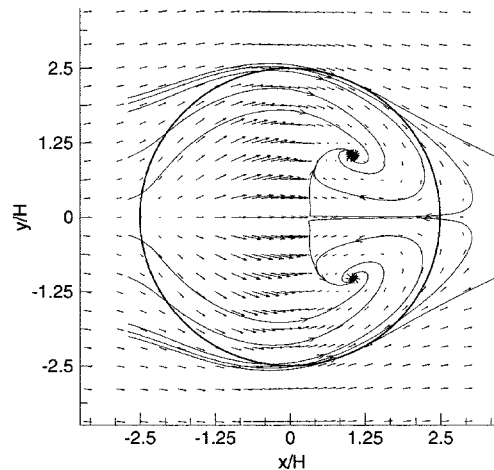


Fig. 8 Mean velocity vectors and flow pattern in the parallel surface of the 3D hill

the near-wall region on the right-hand side of the hill and counterclockwise component on the left-hand side. The velocity field changes rapidly over the hill as the flow separates. The downstream section in a spanwise plane through the rear edge of the hill ($x/H = 2.5$) is shown in Fig. 9b. The transverse flow is broadly inward and downward, but with a rather more complex structure than that in the upstream section. Although there is relatively strong downwash in the upper wake, there is weak upwash. This pattern may be better explained by the distribution of longitudinal vorticity in the section behind the hill, where there is a trailing-vortex pair with central upwash. At the section of $x/H = 10$, the trailing-vortex pair is lifted and weakened, and a lower vortex pair appears outside, but of opposite sense to the trailing-vortex (Fig. 9c).

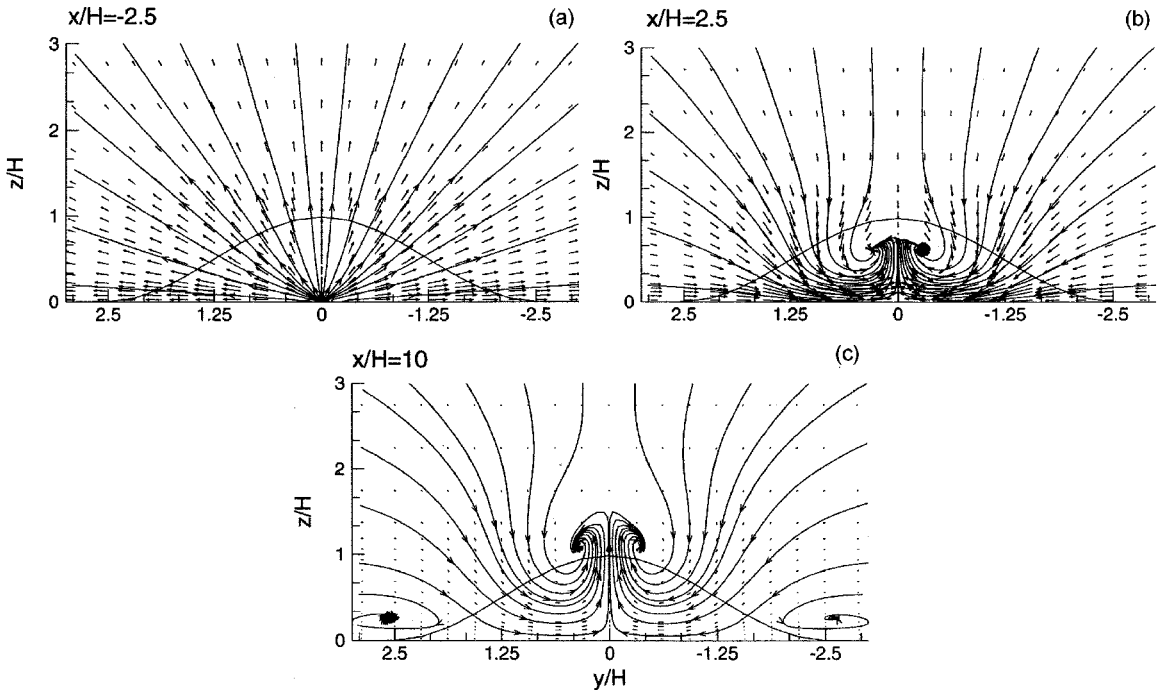


Fig. 9 Mean velocity vectors and flow patterns at (a) $x/H = -2.5$, (b) $x/H = 2.5$ and (c) $x/H = 10$ section

3.3. Turbulence fields

Besides the mean velocity, it is of interest to know how turbulence might be modified as the flow goes over the hill. Turbulence features behind three-dimensional steep hills have not often been investigated using turbulence modelling.

Fig. 10 shows vertical profiles of turbulent kinetic energy in the central plane of the hill. Prediction by Shih's nonlinear model gives better agreement with the experimental value than the standard $k-\epsilon$ model. Especially, in the separated region, the overestimate of the turbulent energy from the standard $k-\epsilon$ model is evidently improved by Shih's nonlinear model. The results on the upstream side of the hill and hilltop are also slightly improved by Shih's model.

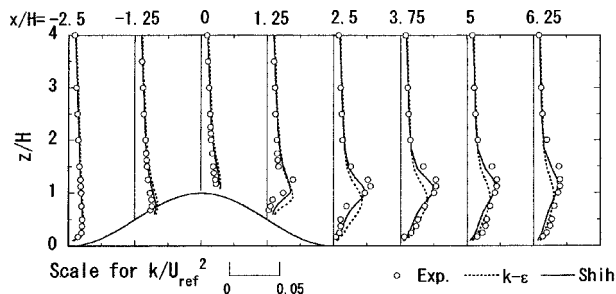


Fig. 10 Comparison of predicted and measured vertical profiles of the turbulent kinetic energy in the central plane of the 3D hill

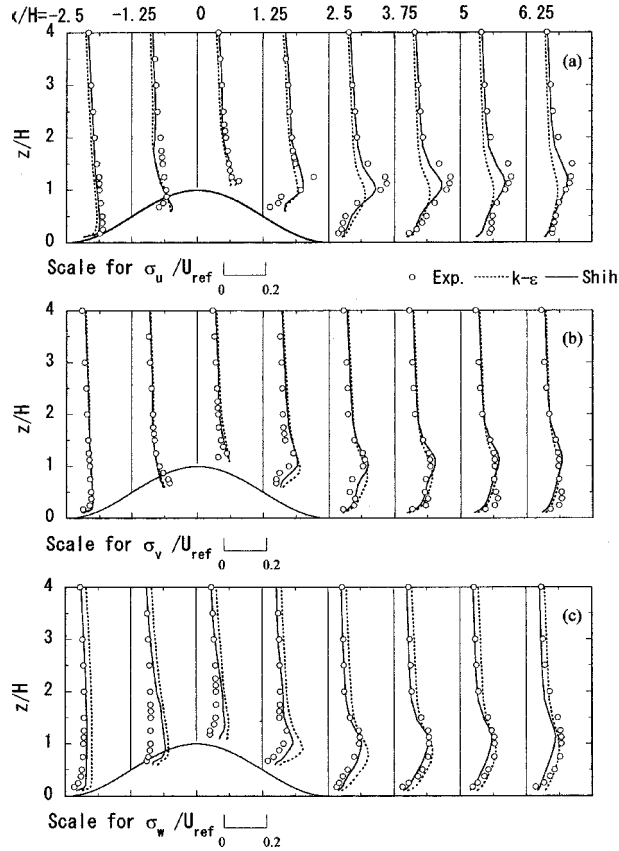


Fig. 11 Comparison of predicted and measured normal stress profiles in the central plane of the 3D hill: (a) streamwise component; (b) spanwise component; (c) vertical component

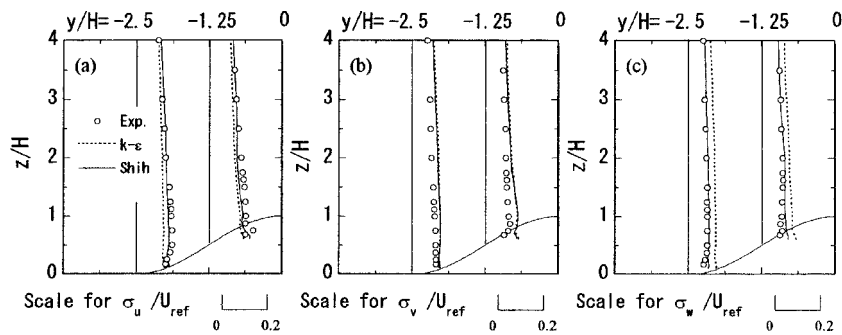


Fig. 12 Comparison of predicted and measured normal stress profiles in the $x/H = 0$ plane: (a) streamwise component; (b) spanwise component; (c) vertical component

The vertical profiles of the three normal stress components in the central plane of the hill are plotted in Fig. 11. As anticipated, the standard $k-\epsilon$ model underestimates σ_u and overestimates σ_w . In contrast, the predictions from the Shih's model reproduce the anisotropy of the normal stress due to the nonlinear terms in Eq. (6), which increase σ_u and decrease σ_w . However, improvement on the

upstream slope of the hill is small. This disagreement seems to be attributed to an inadequate modelling of the turbulence transport terms in Eq. (6), which is a major approximation made in the Reynolds stress algebraic equation models. In this region, the advection of upstream turbulence may have a dominant effect on the turbulence characteristics.

Fig. 12 shows the vertical profiles of the three normal stress components in the $x/H = 0$ plane. Shih's model shows better agreement with the measurements than the standard $k-\varepsilon$ model.

4. Conclusions

A numerical investigation on the turbulent wake flow behind a three-dimensional steep hill has been conducted by using standard $k-\varepsilon$ model and Shih's nonlinear model. The Shih's nonlinear model is found to predict mean flow and turbulence better than the standard $k-\varepsilon$ model and shows good agreement with measurements. Flow patterns behind the circular hill have been carefully examined to explain the features of three-dimensional turbulent wake flows. It is noted that opened streamline pattern is formed in the three-dimensional separated region, while a closed one is revealed in the two-dimensional case. Two vortices, having a three-way-encounter pattern, are also observed on the lee slope of the hill. These vortices cause the flow toward the symmetry-plane and sustain the separation with an opened streamline pattern.

References

- Coelho, P.J. and Pereira, J.C.F. (1992), "Finite volume computation of the turbulent flow over a hill employing 2D or 3D non-orthogonal collocated grid systems", *Int. J. Num. Methods Fluids*, **14**, 423-441.
- Ferreira, A.D., Lopes, A.M.G., Viegas, D.X., and Sousa, A.C.M. (1995), "Experimental and numerical simulation of flow around two-dimensional hills", *J. Wind Eng. Ind. Aerod.*, **54/55**, 173-181.
- Ishihara, T. and Hibi, K. (1998), "An experimental study of turbulent boundary layer over a steep hill", *Proc. of 15th National Sym. on Wind Eng.*, 61-66 [In Japanese].
- Ishihara, T., Hibi, K. and Oikawa, S. (1999), "A wind tunnel study of turbulent flow over a three-dimensional steep hill", *J. Wind Eng. Ind. Aerod.*, **83**, 95-107.
- Ishihara, T. and Hibi, K. (2000), "Numerical simulation of turbulent flow over a steep hill", *J. Wind Eng.*, **83**, 175-188 [In Japanese].
- Jones, W.P. and Launder, B.E. (1972), "The prediction of laminarization with a two-equation model of turbulence", *Int. J. Heat Mass Transfer*, **15**, 301-314.
- Kobayashi, M.H., Pereira J.C.F. and Siqueira, M.B.B. (1994), "Numerical study of turbulent flow over and in a model forest on a 2D hill", *J. Wind Eng. Ind. Aerod.*, **53**, 357-374.
- Kim, H.J., Lee, C.M., Lim, H.C. and Kyong, N.H. (1997), "An experimental and numerical study on the flow over two-dimensional hills", *J. Wind Eng. Ind. Aerod.*, **66**, 17-33.
- Lumley, J. L. (1978), "Computational modeling of turbulent flows", *Adv. Appl. Mech.*, **18**, 124-176.
- Leonard, B.P. (1979), "A stable and accurate convective modelling procedure based on quadratic upstream interpolation", *Comput. Methods Appl. Mech. Eng.*, **19**, 59-98.
- Launder, B.E. and Spalding, D.B. (1974), "The numerical computation of turbulent flows", *Comput. Methods Appl. Mech. Eng.*, **3**, 269-289.
- Patankar, S.V. (1980), *Numerical Heat Transfer and Fluid Flow*, McGraw-Hill, New York.
- Rhie, C.M. and Chow, W.L. (1983), "Numerical study of the turbulent flow past an airfoil with trailing edge separation", *AIAA J.*, **21**, 1525-1532.
- Shih, T.H., Zhu, J. and Lumley, J.L. (1995), "A new Reynolds stress algebraic equation model", *Comput. Methods Appl. Mech. Eng.*, **125**, 287-302.
- Schumann, U. (1977), "Realizability of Reynolds-stress turbulence models", *Phys. Fluids*, **20**, 721-725.
- Utne, T. and Eidsvik, K.J. (1996), "Turbulent flows over mountainous terrain modelled by the Reynolds equations", *Boundary-Layer Meteorol.*, **79**, 393-416.